ACS APPLIED MATERIALS & INTERFACES

Research Article

Cite This: ACS Appl. Mater. Interfaces XXXX, XXX, XXX−XXX

www.acsami.org

Single-Step Synthesis of Magnesium-Doped Lithium Manganese Oxide Nanosorbent and Their Polymer Composite Beads for Selective Heavy Metal Removal

Hitesh Saravaia,* Hariom Gupta,*,† Pooja Popat, Parthrajsinh Sodha, and Vaibhav Kulshrestha

CSIR-Central Salt and Marine Chemicals Research Institute (CSIR-CSMCRI), Council of Scientific & Industrial Research (CSIR), Gijubhai Badheka Marg, Bhavnagar 364002, Gujarat, India

ABSTRACT: Magnesium-doped lithium manganese oxide nanosorbent is prepared by a single-step solid-state method and characterized with appropriate analytical techniques, adsorption kinetic model, and isotherms. Competitive and noncompetitive adsorption studies are performed for a range of heavy metal ions. Prepared nanosorbent has shown explicit selectivity for various heavy metal ions and no remarkable influence of coexisting common interfering ions (Na^+, K^+, Mg^{2+}, and Ca^{2+}), which generally coexist with all natural sources of water, contaminated water, and industrial waste. To achieve easy handling of an adsorbent, polysulfone−nanosorbent (PS−nanosorbent) composite beads are prepared, and their competitive heavy metal removal performance is determined. Competitive adsorption and regeneration studies have shown that PS−nanosorbent beads can be employed for selective heavy metal removal and reuse for multiple cycles.

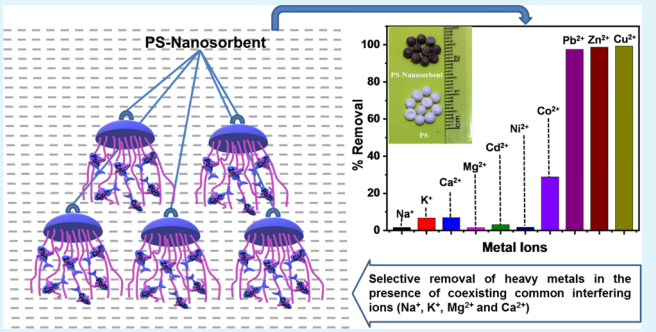

KEYWORDS: *nanosorbent, selective heavy metal removal, magnesium-doped lithium manganese oxide nanostructure, single-step synthesis, solid-state synthesis, polysulfone−nanosorbent composite beads*

1. INTRODUCTION

Industrial discharge is one of the major sources of substantial heavy metal pollutant that seriously affects the quality of water, soil, and ecosystem, leading to a high risk of severe diseases to living animals and plant systems due to their tendency of accumulation into living organism.[1−7] Although few of heavy metals are micronutrients, however, their excess induces severe health complications in humans similarly to other toxic heavy metals. To name some, above the permissible level, copper causes lethargy and anorexia and damages the gastrointestinal tract;[8] cobalt produces goiter and reduces thyroid activity;[9] zinc induces neurological disorders and disrupts iron homeostasis;[10,11] nickel causes respiratory epithelial cell damage and carcinogenic, immunotoxic, skin, and lung cancers;[12−14] lead produces behavioral disorders, kidney damage, anemia, and toxicity;[15] cadmium leads to nephrotoxicity and bone damage;[16] and mercury induces neurological disorders and developmental disabilities, including dyslexia, attention-deficit hyperactivity disorder, and intellectual retardation.[17] WHO has defined the maximum permissible limit for various heavy metals in drinking water, which are 2.00 (Cu) ppm, 0.003 (Cd) ppm, 0.07 (Ni) ppm, 0.01 (Pb) ppm, 3.00 (Zn) ppm, and 0.006 (Hg) ppm.[18] Various approaches for the decontamination of heavy metal from aqueous system have been reported, including ion exchange,[19] adsorption,[20] membrane filtration,[21,22] chemical precipitation,[23] biosorption,[24] and electrochemical methods.[25] Adsorption is one of the simple methods and cost-effective processes for heavy metal removal from contaminated water and waste. Various metal oxide nanostructure-based adsorbents have already been widely applied due to their high surface/volume ratio leading to a good adsorption capability.[26−29] Qu et al. used Fe_3O_4/carboxylate-rich carbon composites for Cu^{2+} removal and showed a comparison with various Fe_3O_4 nanostructure-based adsorbents reported in the literature, which exhibit Cu^{2+} adsorption capacity below 67 mg g^{-1}.[30] Xu et al. prepared iron oxide nanoparticle-immobilized *Phanerochaete chrysosporium* and found their Pb^{2+} removal capacity of 176.3 mg g^{-1}.[31] Recently, amino-functionalized magnetite/kaolin clay has been reported for enhanced removal of Pb^{2+}, Cu^{2+}, and Cd^{2+} with adsorption capacities of 86.6, 16.5, and 22.1 mg g^{-1}, respectively.[32] Zhang et al. reported Fe_3O_4/PANI/MnO_2 core−shell hybrids for the removal of Cd^{2+}, Pb^{2+}, Cu^{2+}, and Zn^{2+} and showed the maximum adsorption of capacity 154 mg g^{-1} for Cd^{2+}.[33] Zhang et al. prepared sulfonated nanoZrO_2/polystyrene for Cu^{+2} removal and found calculated maximum separation capacity of 108 mg g^{-1}; however, a significant reduction in performance in the presence of Mg^{2+} and Ca^{2+} ions is reported.[34] Lithium manganese oxide and their doped derivatives are an excellent cathode material.[35−37] Their protonated forms are also widely reported as ion-sieve system for lithium-ion recovery from aqueous system[38−40] because of

Received: October 1, 2018
Accepted: November 29, 2018
Published: November 29, 2018

DOI: 10.1021/acsami.8b17141
ACS Appl. Mater. Interfaces XXXX, XXX, XXX−XXX

its specific Li selectivity and nonsignificant impact of common interfering ions.[41] So, this type of material can potentially address concern of interference of common ions. Further, Jiang et al., Warner et al., and Lee et al. showed enhanced heavy metal adsorption efficiency with the incorporation of manganese metal either as doping or combining with manganese oxide-type structure.[42−44] Manganese oxide can selectively trap heavy metal ions through electrostatic forces and the formation of strong inner-sphere complexes.[45−51] It suggests a possible potential to lithium manganese oxide and their protonated form-based material for heavy metal separation applications even in the coexisting presence of common interfering ions. Manganese oxide-based materials are available in the literature; however, lithium manganese oxides and their doped structures are almost unexplored in this aspect. Magnesium-doped lithium manganese oxide crystalline structure is comparably more stable as magnesium doping inhibits the degradation/dissolution of crystalline structure against acid desorption.[41,53]

The present work reports a single-step synthesis method for the preparation of magnesium-doped lithium manganese oxide nanosorbent material. Prepared nanosorbent was further protonated to determine its better performing phase (protonated or nonprotonated) for heavy metal removal. Protonated forms of such doped ion-sieve systems are already reported for the recovery of Li^+ metal ions.[38−40] Non-protonated nanosorbent is found to be better and used for all other studies reported in the present work. The effects of pH, sample dose, kinetics, and concentration were studied, and the results were analyzed with kinetic models and adsorption isotherms. The adsorption characteristic of nanosorbent was determined and found to be selective for heavy metal ions (Ni^{2+}, Co^{2+}, Cd^{2+}, Pb^{2+}, Zn^{2+}, Cu^{2+}) with and without the presence of common interfering ions (Na^+, K^+, Mg^{2+}, Ca^{2+}). For easy handling and rapid recovery of adsorbent from adsorbate solution, polysulfone (PS)−nanosorbent composite beads were prepared and studied for heavy metal removal.

2. EXPERIMENTAL METHOD AND CHARACTERIZATIONS

2.1. Materials. Lithium carbonate and manganous acetate tetrahydrate were purchased from Finar Chemicals Limited, India. Lithium chloride anhydrous (extrapure AR) was purchased from Sisco Research Laboratories Pvt. Ltd., India. Magnesium nitrate hexahydrate was purchased from Fisher Scientific India Pvt. Ltd., India. Polysulfone was purchased from Solvay Chemicals, India. $ZnCl_2$, $Pb(NO_3)_2$, $Co(NO_3)_2{\cdot}6H_2O$, and $CaCl_2{\cdot}2H_2O$ were obtained from Merck Chemicals; $MgCl_2{\cdot}6H_2O$ and NaCl were purchased from Fisher Scientific; $CuCl_2{\cdot}2H_2O$, $Cd(NO_3)_2{\cdot}4H_2O$, $NiCl_2{\cdot}6H_2O$, and KCl were obtained from Rankem, SDFCL, Qualigens, and Loba Chemie, respectively.

2.2. Synthesis of Magnesium-Doped Lithium Manganese Oxide. Magnesium-doped lithium manganese oxide (LMMO-400 and LMMO-500) nanostructures were prepared by mixing 302 mg of lithium carbonate, 520 mg of lithium chloride, 5124 mg of manganese acetate, and 2215 mg of magnesium nitrate hexahydrate in a mortar and pestle for 15−20 min, followed by drying and calcination in a muffle furnace at 400 and 500 °C for 5 h. The obtained products were washed five times with deionized water to remove the soluble impurities and dried at 90 °C in an oven. LMMO-400 (prepared at 400 °C) and LMMO-500 (prepared at 500 °C) were stirred with a 0.5 M HCl solution for 24 h to get the protonated samples (HMMO-400 and HMMO-500). To prepare PS−nanocomposite, 500 mg of nanosorbent (LMMO-400) was mixed in 20 mL of chloroform and sonicated for 1 h. Further, 1 g of polysulfone was added slowly to this mixture and stirred for 6 h and sonicated for 1 h to make a homogeneous solution. PS−nanocomposite beads were prepared through phase inversion method by slowly dropping the nano-sorbent−polysulfone homogeneous solution into 20% ethanol−water mixture using a burette with a fine tip. Prepared PS−nanocomposite beads were washed 5−6 times with 20% ethanol−water mixture to remove the solvent and dried in an oven at 90 °C for 8 h.

2.3. Characterization. The phase identification and indexing of the final products were carried out by powder X-ray diffraction (XRD) (Empyrean-PANalytical) operated with Cu Kα radiation in the range of 5−70° (2θ). Fourier transform infrared (FT-IR) results were acquired on a PerkinElmer FT-IR spectrometer by KBr pellet method for nanosorbent, and beads were characterized by attenuated total reflection method using an Agilent Cary 600 series FT-IR spectrometer. Brunauer−Emmett−Teller (BET) surface areas and Barrett−Joyner−Halenda pore size distributions were determined from N_2 adsorption−desorption isotherms acquired using surface area analyzer of Micromeritics. Samples were degassed at 250 °C for 8 h under vacuum before measurement. All transmission electron microscopy (TEM) images and scanning transmission electron microscopy (STEM)/energy dispersive X-ray spectroscopy (EDS) elemental maps were acquired by transmission electron microscopy (TEM of JEOL JEM); all scanning electron microscopy (SEM) imaging and elemental mapping were done by imaging and scanning electron microscopy/energy-dispersive X-ray spectroscopy (SEM/EDS), respectively, by field emission scanning electron microscopy (FE-SEM, Jeol JSM 7100F). Thermogravimetric (TG) analyses were carried out on METTLER TOLEDO STAR SW at a heating rate of 10 °C min^{-1} in the range of room temperature to 900 °C using N_2 gas. Quantification of metal ion concentration for all adsorption experiments was performed with inductively coupled plasma optical emission spectrometry PerkinElmer (ICP Optima 2000 DV).

2.4. Adsorption Characteristics of Nanosorbent and PS−Nanosorbent Composite Beads. *2.4.1. Comparative Adsorption Performance of Prepared Nanosorbents.* The prepared magnesium-doped lithium manganese oxide nanosorbents (LMMO-400, LMMO-500) and their protonated samples (HMMO-400, HMMO-500) are used for Cu^{2+} ions adsorption study to identify the nanosorbent of better efficacy. All adsorption experiments for these nanosorbents are performed with a Cu^{2+} solution of 200 ppm and a sorbent dose of 1 g L^{-1} for an adsorption time of 6 h. The LMMO-400 is chosen for all further study due to its better adsorbing capability.

2.4.2. Effect of pH Variation. The effect of pH variation in the range of 1−6 has been studied by stirring the 0.25 g L^{-1} LMMO-400 adsorbent with a 40 ppm Cu^{2+} solution for 6 h.

2.4.3. Effect of Nanosorbent Dose. Nanosorbent dose study was performed to reveal the adsorption behavior of the LMMO-400 dose in Cu^{2+} containing aqueous media. The experiments were carried out using 0.5−3.0 g L^{-1} of LMMO-400 sample doses with 40 ppm of the Cu^{2+} solution and stirred for 6 h. The amount of metal ions adsorbed on prepared nanosorbents was determined by the following equation

$$q_e = (C_0 - C_e)\frac{V}{w}$$

where C_0 and C_e are the initial and final concentrations of metal ion, respectively. V is the volume of metal solution, and w is the adsorbent mass used in adsorption experiments.

2.4.4. Adsorption Experiments for Kinetics and Isotherm Study. For kinetic study, a time-dependent adsorption experiment was performed with a nanosorbent dose of 0.25 g L^{-1} and 20 ppm Cu^{2+} solution under stirring for different intervals of time (3, 5, 15, 30, 60, 120, 240, 360, 480, 960, 1440, and 2400 min). Obtained adsorption results were fitted in with pseudo-first-order, second-order, and intraparticle diffusion models to describe the kinetic characteristics of the nanosorbent material. For isotherm, adsorption experiments were carried out at a fixed nanosorbent dose of 2.0 g L^{-1} and different concentrations of adsorbate solution (Cu^{2+}: 25−500 ppm) under stirring for 24 h. The obtained results were fitted with the Langmuir and Freundlich adsorption isotherms.

DOI: 10.1021/acsami.8b17141
ACS Appl. Mater. Interfaces XXXX, XXX, XXX−XXX

2.4.5. Effect of Interfering Metal Ions on the Adsorption Capacity of Nanosorbent. The effect of these interfering metal ions (Na^+, K^+, Mg^{2+}, and Ca^{2+}) on the adsorption capacity of nanosorbent for heavy metal ion (Cu^{2+} ion) was investigated with 200 ppm Cu^{2+} concentration present in three different matrices NKCM-200, NKCM-500, and NKCM-2000 of interfering ions. These matrices are aqueous solutions containing 200, 500, and 2000 ppm concentrations of each interfering ion (Na^+, K^+, Ca^{2+}, and Mg^{2+}), respectively.

2.4.6. Determination of Adsorption Capacity of Heavy Metal Ions Performed Individually. Individual metal ion adsorption experiments were carried out with a nanosorbent dose of 2 g L^{-1} and an adsorbate solution of 200 ppm concentration of individual metal ions (Na^+, K^+, Ca^{2+}, Mg^{2+}, Cu^{2+}, Pb^{2+}, Zn^{2+}, Cd^{2+}, Co^{2+}, and Ni^{2+}) under stirring for a time span of 24 h.

2.4.7. Adsorption Study of Nanosorbent for Mixed Matrix System of Heavy Metal Ions in the Presence and Absence of Common Interfering Ions (Na^+, K^+, Ca^{2+}, Mg^{2+}). To prepare 20 ppm mixed matrix, appropriate amounts of heavy metal salts corresponding to each ion (Cu^{2+}, Pb^{2+}, Zn^{2+}, Cd^{2+}, Co^{2+}, Ni^{2+}) are mixed together to achieve 20 ppm concentration of each individual ion into the mixture. The selectivity heavy metal adsorption performance of nanosorbent from this prepared 20 ppm mixed matrix was evaluated in the absence and presence of 200 ppm concentration of common interfering ions (Na^+, K^+, Ca^{2+}, Mg^{2+}) with a nanosorbent dose of 2 g L^{-1} for the adsorption time of 24 h.

2.4.8. Adsorption and Desorption Study of PS–Nanosorbent Composite Beads. The prepared polysulfone (PS) and PS–nanosorbent composite beads were applied for the heavy metal adsorption from mixed matrix of heavy metal in the presence of common interfering ions. Adsorption experiment was performed with 8 g L^{-1} (equivalent to nearly 2 g L^{-1} nanosorbent in PS–nanosorbent bead) dose of PS and PS–nanosorbent beads with mixed matrix of heavy metal and common ions (Na^+, K^+, Ca^{2+}, Mg^{2+}, Cu^{2+}, Pb^{2+}, Zn^{2+}, Cd^{2+}, Co^{2+}, Ni^{2+}) for an adsorption time span of 24 h. The desorption kinetics of these beads were performed in a 0.5 M HCl solution with a sample dose of 20 g L^{-1}.

2.4.9. Recyclability of PS–Nanosorbent Composite. The recyclability of PS–nanosorbent composite beads was performed by adsorbing the heavy metal ions same as Section 2.4.9, and desorption of heavy metals was carried out by stirring the composite beads for 480 min using a 0.5 M HCl solution with a 20 g L^{-1} sample dose. The 0.2 M $NaHCO_3$ solution was used for the surface neutralization of the acid-treated beads at each cycle.

3. RESULTS AND DISCUSSION

3.1. Characterization of Nanosorbents. The XRD patterns of magnesium-doped lithium manganese oxide (LMMO) nanostructures prepared at 400 and 500 °C and their corresponding protonated LMMO (HMMO) are shown in Figure 1. All major diffraction peaks are well indexed to the (111), (311), (222), (400), (331), (511), (440), and (531) planes of crystalline cubic spinel structure of magnesium-doped lithium manganese oxide (JCPDS card no. 04-007-4348). The diffraction peak marked with "*" is assigned to Mn_2O_3 (JCPDS card no. 00-031-0825), which disappears in protonated samples due to dissolution of Mn_2O_3 in protonation process.[52] The Scherrer equation was employed to calculate the crystallite size, which was found to be 18 nm for LMMO-400, 33 nm for LMMO-500, 18 nm for HMMO-400, and 30 nm for HMMO-500 corresponding to diffraction peak of the (111) plane. The increase of crystallite size with the increase of temperature is possibly due to enhancement of nucleation rate with temperature. Figure 2 represents TEM images and lattice lines of nanosorbent prepared at 400 °C (LMMO-400) and 500 °C (LMMO-500). It shows the formation of cubic crystalline particles of nanometer size for

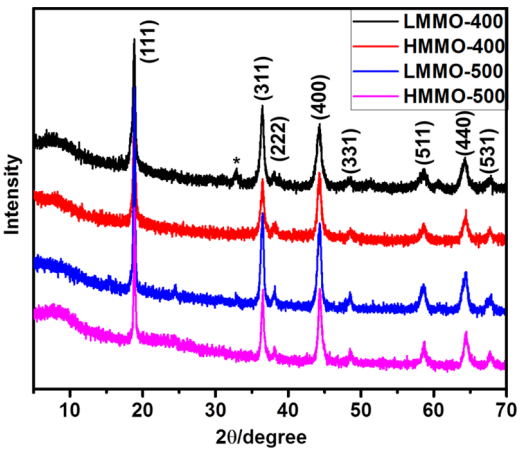

Figure 1. XRD patterns of the synthesized magnesium-doped lithium manganese oxide at 400 and 500 °C with their corresponding protonated samples.

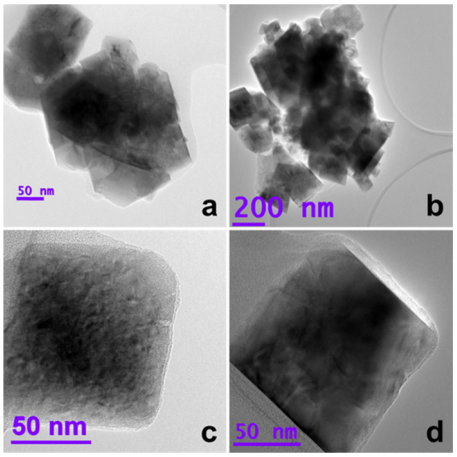

Figure 2. TEM images of nanosorbent: LMMO-400 (a, c) and LMMO-500 (b, d).

both samples; however, slightly larger size is observed for LMMO-500, which is consistent with the trend of crystallite size measured in XRD.

Fourier transform infrared (FT-IR) spectra of prepared LMMOs nanosorbent and their protonated (HMMOs) samples are presented in Figure 3. The characteristic peaks of MnO stretching of MnO_6 group are found at about 510 and 635 cm^{-1}.[53] A shoulder at 450 cm^{-1} is attributed to MgO stretching, which confirms the formation of Mg-doped nanostructure.[54] An IR band at 1625 cm^{-1} is assigned to the bending mode of water molecules and C=O of carbonate group bound on the surface of nanostructure. A weak peak at 1475 cm^{-1} is assigned to the –C–O stretching of carbonate group attached to nanostructure.[55] Surface area of prepared nanosorbents is characterized through the BET adsorption–desorption isotherm. Its values are found to be 11.16 for LMMO-400 and 3.78 m^2 g^{-1} for LMMO-500. Smaller surface area for nanosorbent prepared at higher temperature is due to its relatively large particle size as described in TEM and XRD results. Particle size and surface area of our prepared LMMO-400 nanosorbent are in good agreement with lithium manganese oxide nanoparticle (50–100 nm; 14 m^2 g^{-1}) reported previously by Shaju et al.[56]

DOI: 10.1021/acsami.8b17141
ACS Appl. Mater. Interfaces XXXX, XXX, XXX–XXX

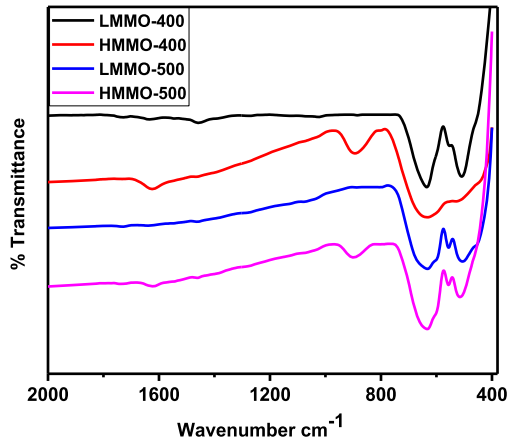

Figure 3. FT-IR spectra of LMMOs prepared at 400 and 500 °C and their corresponding protonated samples.

3.2. Adsorption Study. The comparative Cu^{2+} ion adsorption efficacy of magnesium-doped lithium manganese oxide nanosorbent (LMMO-400, LMMO-500) and their protonated samples (HMMO-400, HMMO-500) performed for a nanosorbent dose of 1 g L^{-1} and an adsorption time of 6 h are shown in Figure 4, which reveals a far better adsorption

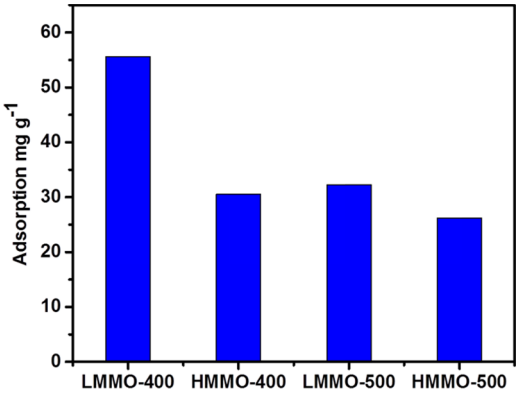

Figure 4. Adsorption capacity graph comparing adsorbing capability of prepared nanosorbent evaluated for the adsorption time of 6 h.

efficacy to LMMO-400 nanosorbent. It is due to relatively higher surface area providing more adsorbing sites to LMMO-400 in comparison to LMMO-500. The reduced performance for their corresponding protonated nanosorbents is possibly due to the variation in their crystalline structure and surface properties. The LMMO-400 is chosen for all further study due to its better adsorbing capability.

3.2.1. Effect of Sample Dose. Figure 5 shows the effect of nanosorbent (LMMO-400) doses (0.5, 1.0, 1.5, 2.0, 2.5, and 3.0 g L^{-1}) on the removal of Cu^{2+} ions using 40 ppm Cu^{2+} solution for 6 h. The % removal of Cu is found to increase with the increase of nanosorbent dose as the adsorption sites are increased.[38] The enhancement in the Cu^{2+} removal was achieved from 43.90 to 99.22% with sample doses of 0.5 and 2 g L^{-1}, respectively. Almost 100% removal of Cu^{2+} has been achieved with a nanosorbent dose of 2.0 g L^{-1} from a 40 ppm Cu^{2+} solution in a time span of 6 h; 100% Cu removal can be obtained by a nanosorbent dose of 0.04 g L^{-1} per ppm of Cu.

3.2.2. Influence of pH. The effect of adsorbate solution pH on heavy metal (Cu^{2+} ions) adsorption efficiency of nano-

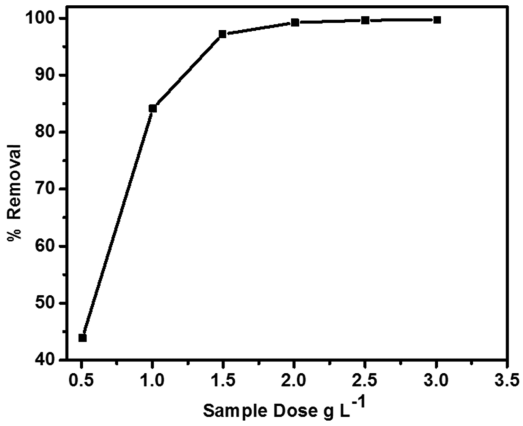

Figure 5. Nanosorbent dose characteristics performed for Cu solution for an adsorption time of 6 h.

sorbent was performed with an adsorbent dose of 0.25 g L^{-1} using a 40 ppm Cu^{2+} solution for the adsorption time of 6 h, and results are shown in Figure 6. The adsorption capacity is

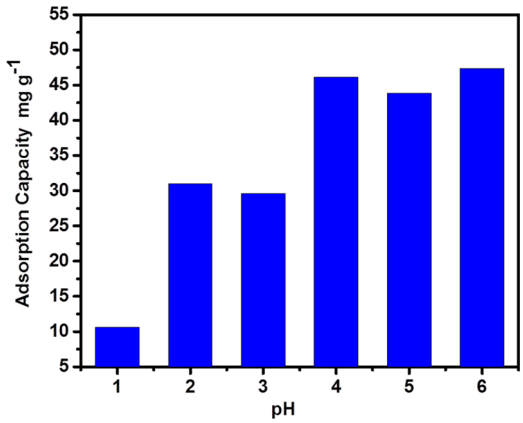

Figure 6. Effect of adsorbate solution pH on adsorption capacity of nanosorbent.

found to increase up to pH 4 and be almost unchanged in the pH range of 4−6. Ge et al. reported a similar trend of heavy metal removal efficiency for nanomaterials, which is same in trend as reported for heavy metal removal by nanomaterial.[57] The pH of Cu^{2+} solution of concentration ranging from 10 to 200 ppm lies within 5.75−5.24. It suggests that no pH adjustment is required for the examined range of Cu^{2+} ion concentration as it falls in the range of 4−6.

3.2.3. Effect of Adsorption Time and Kinetic Model Study. The kinetic adsorption responses for the dose of 0.25 g L^{-1} and 20 ppm Cu^{2+} adsorbate concentration are represented in Figure 7, which show an increase in adsorption capacity with time. These adsorption responses are fitted with pseudo-first-order (eq 1), pseudo-second-order (eq 2), and intraparticle diffusion (eq 3) adsorption models,[58,59] and their results are shown in Table 1. The fitting parameter R^2 for the pseudo-second-order model is closer to 1, reflecting the better fitting of model with experimental data. However, other fitted model results do not meet the fitment criteria and also not consistent with the experimental results. It attributes that copper (heavy metal) adsorption follows pseudo-second-order adsorption pathway

DOI: 10.1021/acsami.8b17141
ACS Appl. Mater. Interfaces XXXX, XXX, XXX−XXX

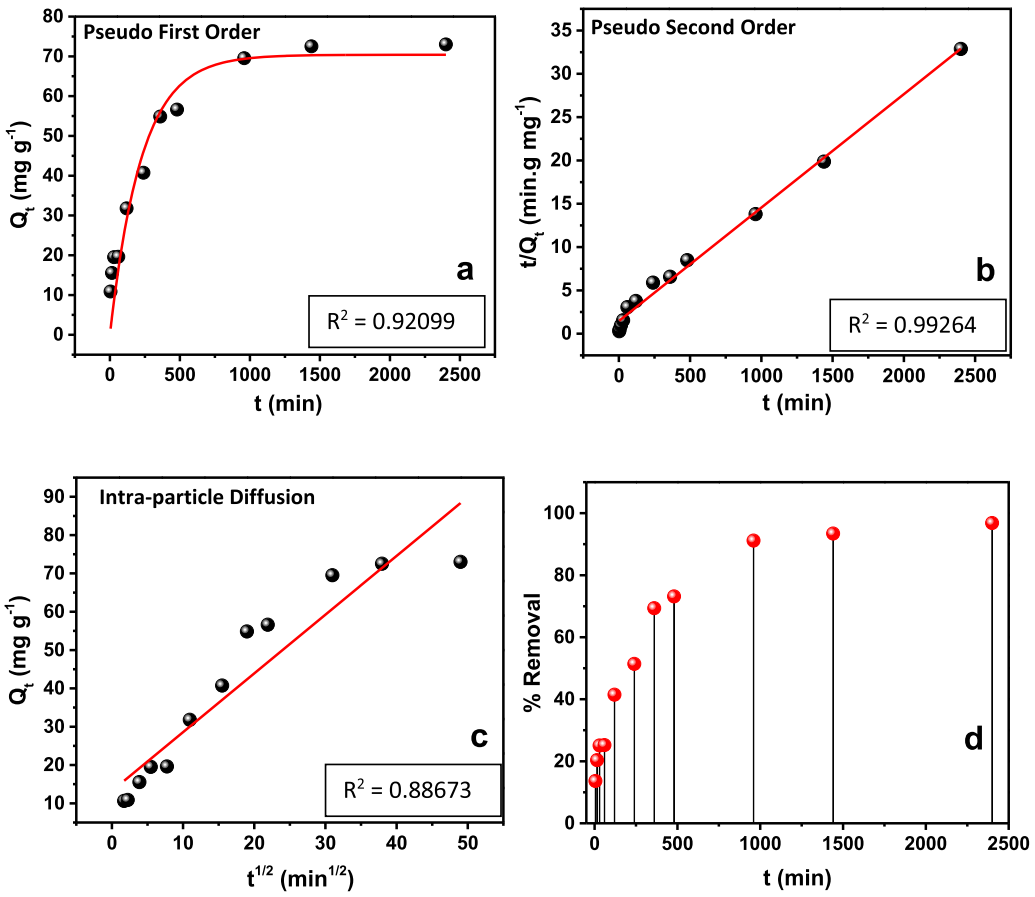

Figure 7. Kinetic study for adsorption responses of nanosorbent at different time intervals: (a) pseudo-first-order, (b) pseudo-second-order, (c) intraparticle diffusion fitting results, and (d) time-dependent removal efficiency.

Table 1. Parameters of Kinetic Model for the Adsorption of Cu^{2+} (Heavy Metal) Ion on Nanosorbent

kinetic model	parameters	Cu(II)
pseudo-first-order	Qe_1 (mg g^{-1})	70.395
	K_1 (min^{-1})	0.442 × 10^{-2}
	R^2	0.92099
pseudo-second-order	Qe_2 (mg g^{-1})	76.3358
	K_2 (g mg^{-1} min^{-1})	0.11775 × 10^{-3}
	h (mg g^{-1} min^{-1})	0.68614
	R^2	0.99264
intraparticle diffusion	K_{id} (mg g^{-1} min$^{-1.5}$)	1.533
	C (mg g^{-1})	13.23946
	R^2	0.88673

$$q_t = q_e(1 - e^{-K_1 t}) \quad (1)$$

$$\frac{t}{q_t} = \frac{1}{K_2 q_e^2} + \frac{t}{q_e} \quad (2)$$

$$q_t = K_{id} t^{1/2} + C \quad (3)$$

where q_e and q_t are the adsorption capacities (mg g^{-1}) on the adsorbent at equilibrium and at time t, respectively; K_1 (min^{-1}) and K_2 (g mg^{-1} min^{-1}) are the rate constants for pseudo-first-order and pseudo-second-order adsorption kinetics; K_{id} (mg g^{-1} min$^{-1/2}$) is the intraparticle diffusion rate constant; and C is a constant.

3.2.4. Effect of Adsorbate Concentration and Adsorption Isotherm. The adsorption nature of adsorbate on the adsorbent is determined through fitting of adsorption experimental data to Langmuir and Freundlich isotherm models. Langmuir isotherm is a monolayer adsorption model. It is based on the assumption that adsorption sites are identical and energetically equivalent. Langmuir isotherm is expressed mathematically by eq 4

$$\frac{C_e}{q_e} = \frac{1}{q_m K_L} + \frac{C_e}{q_m} \quad (4)$$

where q_e and q_m are the amount of heavy metal ions adsorbed at equilibrium concentration and maximum adsorption capacity in mg g^{-1}, respectively; C_e is the equilibrium concentration of heavy metal ions in mg L^{-1}; and K_L is the Langmuir constant.

However, Freundlich isotherm assumes and describes the multilayer adsorption process on the heterogeneous surface. It can be represented mathematically by eq 5

$$\ln Q_e = \ln K_F + \frac{1}{n} \ln C_e \quad (5)$$

Isotherm model fittings are shown in Figure 8, and the obtained isotherm parameters along with correlation coefficient (R^2) are listed in Table 2. The experimental data are found to be best fitted to Langmuir model compared to Freundlich model, and its correlation coefficient is relatively close to unity. It attributes the monolayer adsorption nature for

DOI: 10.1021/acsami.8b17141
ACS Appl. Mater. Interfaces XXXX, XXX, XXX−XXX

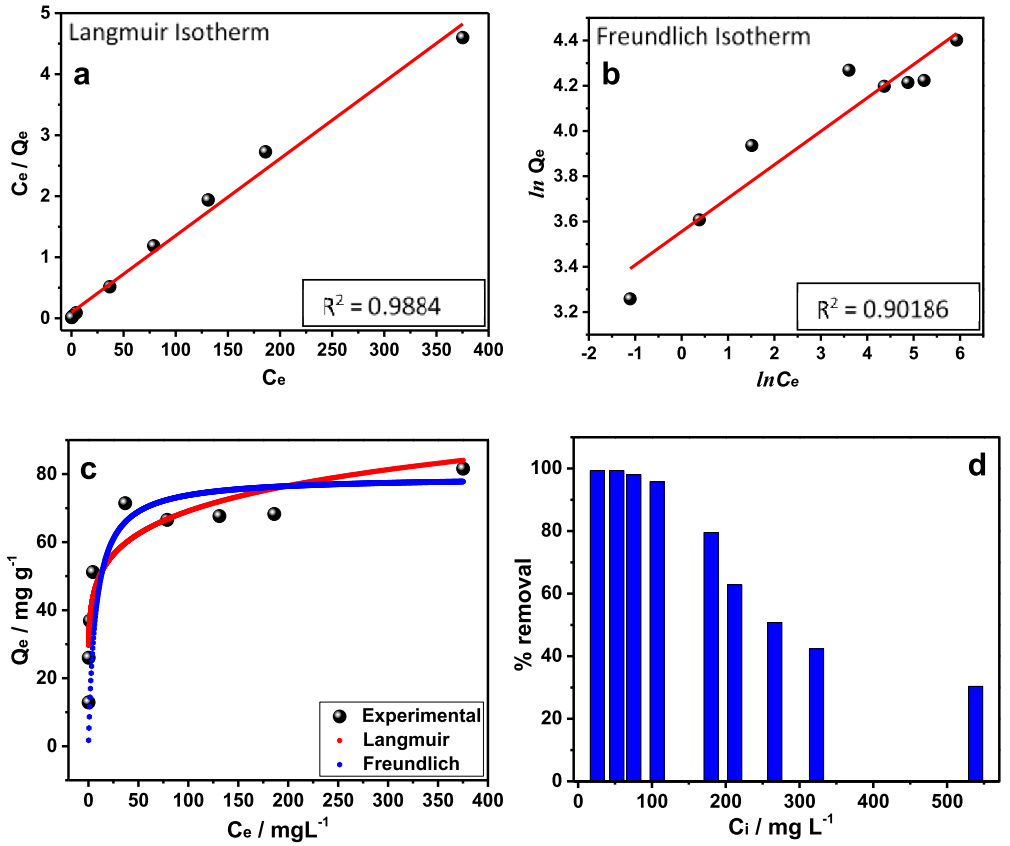

Figure 8. (a) Langmuir and (b) Freundlich adsorption isotherms and their (c) fitting comparison and (d) % removal efficiency at different concentrations.

Table 2. Isotherm Parameters of Cu Heavy Metal Adsorption on Nanosorbent

isotherm	parameters	Cu(II)
Langmuir model	Q_m (mg g^{-1})	79.37
	K_L (L mg^{-1})	0.1326
	R^2	0.9884
Freundlich model	K_F ((mg g^{-1}) (L $mg^{-1})^{1/n}$)	35.0881
	n	6.77
	R^2	0.9018

bivalent heavy metal ions on nanosorbent. The maximum adsorption capacity estimated using Langmuir model is in good agreement with the experimental result and found to be 79.37 mg g^{-1}. The percentage removal of Cu^{2+} from aqueous solutions of 25−100 ppm concentration range is found to be greater than 99−95% for the adsorbent dose of 2.0 g L^{-1}, as shown in Figure 8. It reveals that greater than 95% removal level can be achieved with the dose of 1.0 g L^{-1} per 50 ppm concentration of Cu^{2+} in solution.

The separation feasibility of nanosorbent for heavy metal has been predicted through separation factor or equilibrium parameter (R_L) as described in eq 6 using the essential feature of Langmuir isotherm (K_L)

$$R_L = \frac{1}{(1 + K_L C_i)} \tag{6}$$

where C_i is the initial concentration of metal ions in adsorbate solution in mg L^{-1} and K_L is the Langmuir constant. The separation factor (R_L) value describes the type of Langmuir isotherm to be linear (R_L = 1), favorable (0 < R_L < 1), unfavorable (R_L > 1), and irreversible (R_L = 0).[60] R_L values for all examined initial concentrations of heavy metal ion used in Langmuir isotherm and a nanosorbent dose of 2 g L^{-1} are found to be in the range of 0.0138−0.2250, which indicates that nanosorbent is the favorable material for the separation of heavy metal ions.

3.2.5. Effect of Common Interfering Metal Ions. Common interfering metal ions (Na^+, K^+, Mg^{2+}, Ca^{2+}) are generally present in almost all natural sources of water (i.e., river, lake, ocean, and groundwater), industrial waste, and contaminated water. These ions are the most common interfering ions in the process of removal of heavy metal contaminants, which leads to a drastic attenuation in the removal efficiency of adsorbent materials and process. The effect of these interfering metal ions (Na^+, K^+, Mg^{2+}, and Ca^{2+}) on the adsorption capacity of nanosorbent for Cu^{2+} heavy metal ion has been examined with 200 ppm Cu^{2+} concentration present in three different matrices NKCM-200, NKCM-500, and NKCM-2000. These matrices are aqueous solutions containing 200, 500, and 2000 ppm concentrations of each interfering ion (Na^+, K^+, Mg^{2+}, and Ca^{2+}), respectively. Nanosorbent does not show significant variation in adsorption capacity on increasing the concentration of interfering common ions (Figure 9). Its adsorption capacity is found to be well consistent with the results of adsorption experiment performed in the previous section without interfering metal ions. It attributes a novel adsorption characteristic of nanosorbent for Cu^{2+} heavy metal ion even at quite high concentration of interfering ions. Adsorption and distribution of adsorbed Cu^{2+} ions on nanosorbent is evaluated with STEM/EDS and SEM/EDS elemental mapping analyses; results are shown in Figure 10. STEM elemental mapping

DOI: 10.1021/acsami.8b17141
ACS Appl. Mater. Interfaces XXXX, XXX, XXX−XXX

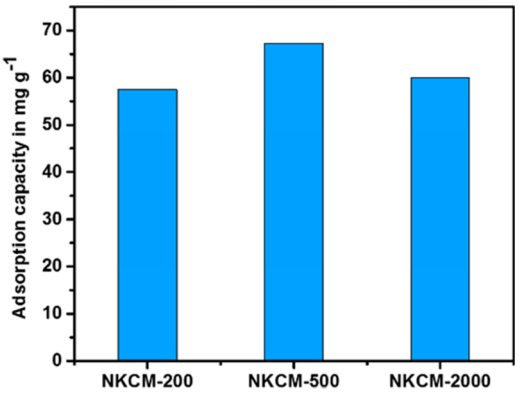

Figure 9. Performance of Cu^{2+} adsorption in the presence of different Na^{+}, K^{+}, Ca^{2+}, and Mg^{2+} concentrations.

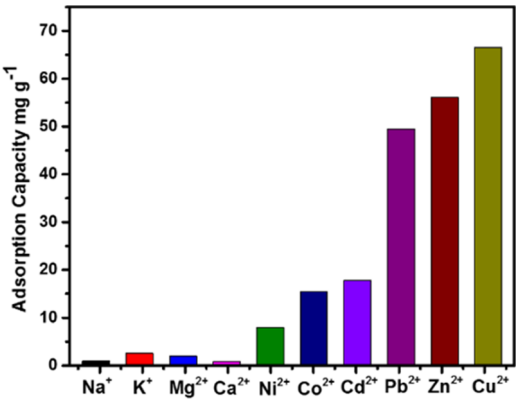

Figure 11. Comparative adsorption characteristics of nanosorbent for various heavy metal ions and common interfering ions performed individually.

represents well-distributed Cu^{2+} ions over the surface of nanosorbent particles, which disclose the availability of active adsorbing sites throughout the surface of the adsorbent particle. Further, a uniform presence of adsorbed Cu^{2+} ions over the nanosorbent in SEM/EDS elemental mapping relates the formation of adsorbent particles of identical adsorbing characteristics.

3.2.6. Adsorption Characteristics for Heavy Metal and Interfering Metal Ions. To further investigate the capability of nanosorbent for other heavy metal and interfering metal ions, comparative adsorption characteristics of nanosorbent for various heavy metal ions (Ni^{2+}, Co^{2+}, Cd^{2+}, Pb^{2+}, Zn^{2+}, and Cu^{2+}) and common interfering metal ions (Na^{+}, K^{+}, Mg^{2+}, and Ca^{2+}) have been investigated and are shown in Figure 11. It shows a specific selectivity for heavy metal ions with the selectivity order of $Ni^{2+} < Co^{2+} < Cd^{2+} < Pb^{2+} < Zn^{2+} < Cu^{2+}$; however, the adsorption response for the common interfering metal ions is found to be negligible or nonsignificant in comparison to heavy metal ions. The adsorption capacity of our prepared nanosorbent is compared to other adsorbents for heavy metal previously reported in the literature (Table 3), which is well competitive and even better for some ions in comparison to various reported adsorbents.

Adsorption responses of nanosorbent for mixed matrix of all examined heavy metal ions in the absence and presence of common interfering ions are illustrated in Figure 12. It shows almost same selectivity trend and nearly complete removal capability for three heavy metal ions (Pb^{2+}, Zn^{2+}, and Cu^{2+}); however, slight adsorption deterioration is observed in the presence of relatively high concentration of common interfering metal ions. Therefore, it can be concluded that prepared nanosorbents have good potential to remove a number of heavy metal ions together from the mixed aqueous matrix of heavy metal ions even in the presence of a relatively high concentration of common interfering ions, and such mixed matrix studies are either rarely or less reported for other types of heavy metal adsorbents.

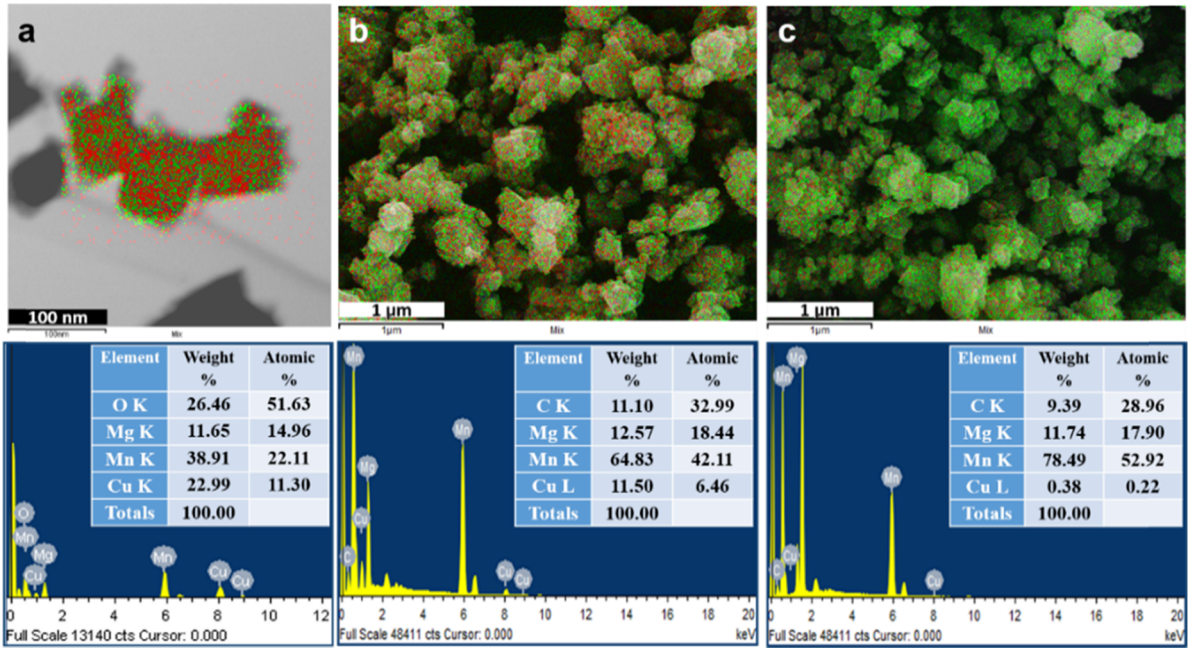

Figure 10. Elemental mapping and EDS analyses of copper adsorbed (STEM/EDS: a, SEM/EDS: b) and without copper adsorbed (SEM/EDS: c) nanosorbent; red: Cu, green: Mg.

DOI: 10.1021/acsami.8b17141
ACS Appl. Mater. Interfaces XXXX, XXX, XXX−XXX

Table 3. Comparison of Heavy Metal Adsorption Capacity on Prepared Nanosorbent with Other Reported Adsorbents

adsorbents	adsorption capacity in mg g^{-1}						references
	Cu^{2+}	Pb^{2+}	Zn^{2+}	Cd^{2+}	Ni^{2+}	Co^{2+}	
formulated zeolite-portland cement mixture portland cement mixture	23.25	27.03	12.85	10.87			61
hexadentate ligand-modified magnetic nanocomposites	78.67	11.31		13.88	7.64	4.86	62
alkaline-treated peat		6.89			5.57	7.11	63
thioacetamide chemically immobilized on silica gel	21.01	20.04		17.76			64
NH_2-MCM-41 mesoporous silica powders				79.8	40.5		65
cellulose/chitin beads	32.4	176.1		69.7			66
Fe_3O_4/carboxylate-rich carbon composite	66.67						30
carboxymethyl-β-cyclodextrin-conjugated magnetic nanoparticles	47.2						67
lignin/MgO−SiO_2 hybrid	83.98						68
MnO_2-modified graphite sorbents from spent Li-ion batteries		99.88		29.49			28
PVP-coated $ZnMoS_4$ nanoparticles	130						69
amino-functionalized magnetite/kaolin clay	16.5	86.1		22.1			32
3-aminopropyltriethoxysilane and glutaraldehyde-modified Fe_3O_4 nanoparticles	61.07						70
poly(amic acid) vesicle	61.1	206.3	64.8		58.6		1
Fe_3O_4/MnO_2 nanocomposite				53.2			71
carboxymethyl-β-cyclodextrin polymer-modified Fe_3O_4 nanoparticle		64.5		27.7	13.2		72
nanosorbent (LMMO-400)	66.54	49.46	56.15	17.80	7.94	15.42	present study

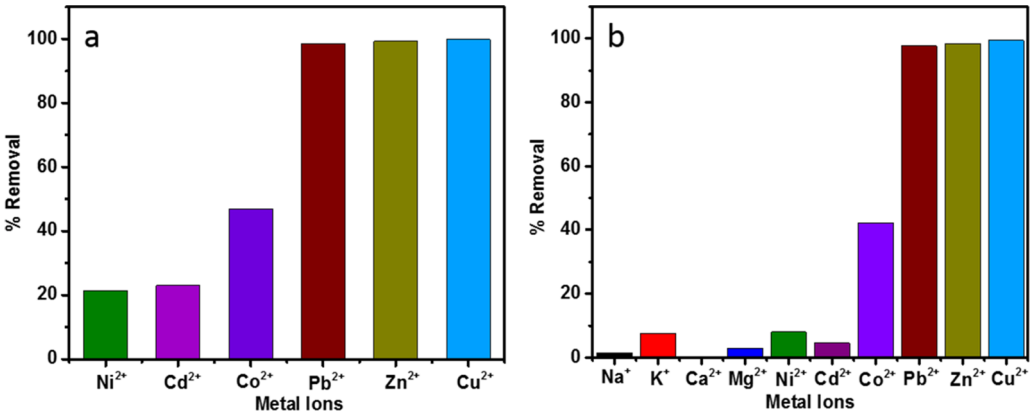

Figure 12. Heavy metal removal performance of nanosorbent from the mixed solution of heavy metal ions in the absence (a) and presence of common interfering ions (b).

3.2.7. Polymer−Nanosorbent Composite and Its Adsorption Performance. Nanosorbent is composed of particles of nanometer size. After adsorption, rapid removal of these nanosized particles from aqueous adsorbate solution is still a challenging process; sometimes, it is not possible to recover all of the particles of nanosorbent from the aqueous adsorbate solution. Therefore, it is an essential need to resolve this issue associated with nanosorbent for its better and realistic heavy metal removal application. To address this aspect, polysulfone−nanosorbent (PS−nanosorbent) composite beads are prepared, which can be easily handled and rapidly recovered from the adsorbate solution. The characterization results of PS and prepared PS−nanosorbent composite beads are shown in Figure 13; an increase in the intensity of FT-IR peak at regions about 500 and 636 cm^{-1} (characteristic peak position of prepared nanosorbent) for PS−nanocomposite attributes the presence of nanosorbent in PS matrix. SEM/EDS results confirm the formation of uniformly nanosorbent distributed PS composite beads.

Adsorptive removal potential and reusability of PS−nanosorbent beads were studied with the mixed solutions of heavy metals in the presence of common interfering ions, and results are shown in Figure 14. Pure PS beads have shown a negligible or nonsignificant adsorption for heavy metal ions. However, PS−nanosorbent beads have disclosed a competitive selectivity for Pb^{2+}, Cu^{2+}, and Zn^{2+} in comparison to other heavy metals (Figure 14a). Desorption kinetics (Figure 14c,d) is found to closely follow the pseudo-second-order desorption pathway with R^2 values of 0.9966, 0.9157, and 0.9862 for Cu^{2+}, Pb^{2+}, and Zn^{2+} ions, respectively, which are in good agreement with previously reported desorption kinetics in acidic media.[73] Figure 14b illustrates a significant potential toward reusability of these beads for multiple cycles with some compromise in performance. These results attribute that PS−nanosorbent beads can selectively remove Pb^{2+}, Cu^{2+}, and Zn^{2+} ions and be used for multiple cycles; however, nanosorbent individually can separate a wide range of heavy metal ions. This compromise is possibly due to the competitive and polymer hindrance on the sites responsible for the adsorption of other heavy metal ions. Adsorption and recyclability performance of prepared nanosorbent may be further improved with nanosorbent composite system of different polymers.

4. CONCLUSIONS

Magnesium-doped lithium manganese oxide nanosorbents are prepared successfully by a single-step solid-state method.

DOI: 10.1021/acsami.8b17141
ACS Appl. Mater. Interfaces XXXX, XXX, XXX−XXX

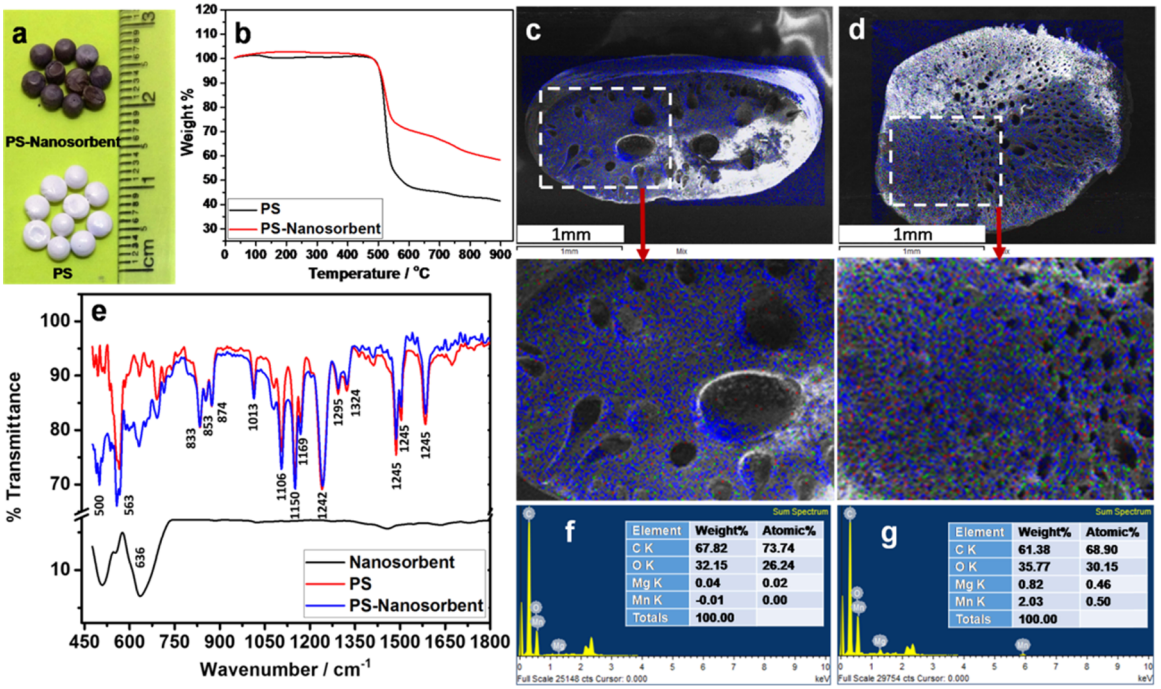

Figure 13. Characterization of prepared PS and PS−nanosorbent composite beads: (a) optical appearance, (b) TG analysis, (c, f) SEM/EDS elemental mapping analysis of PS, (d, g) SEM/EDS elemental mapping analysis of PS−nanosorbent with map color blue, red, and green for C, Mn, and Mg elements, respectively, and (e) FT-IR analysis.

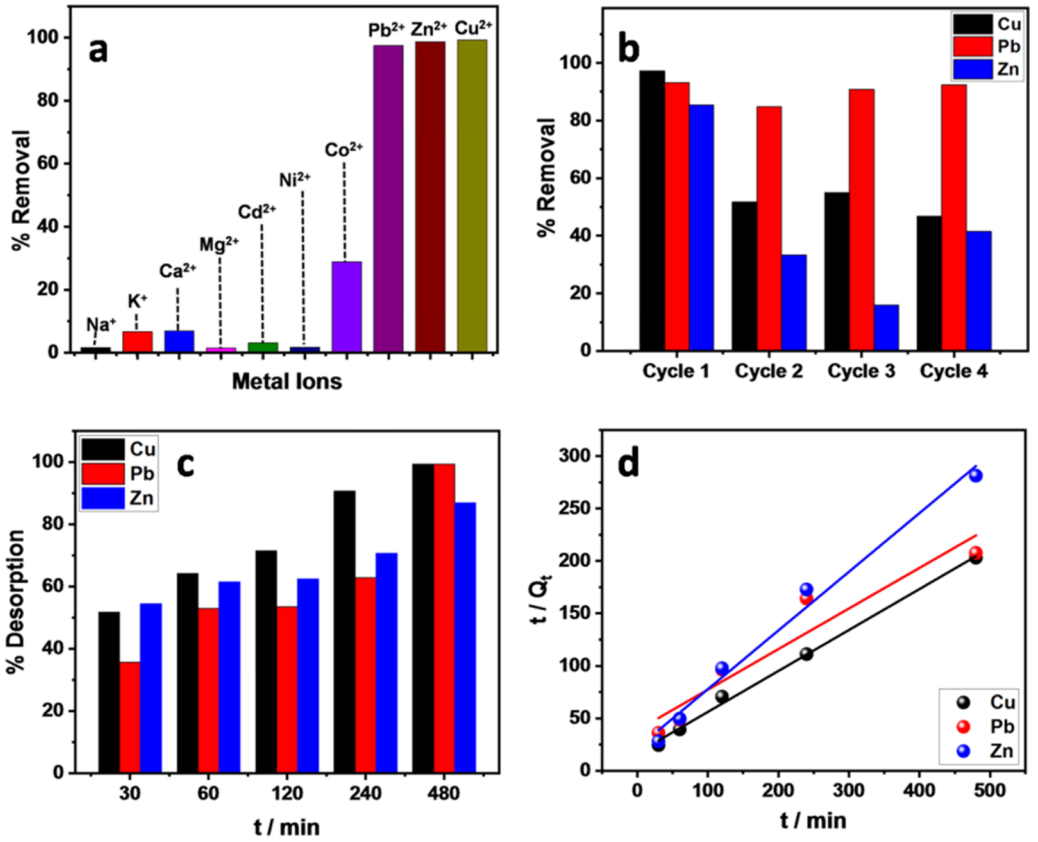

Figure 14. Representing adsorption performance (a), reusability performance (b), and desorption kinetic (c, d) of PS−nanosorbent beads.

Prepared nanosorbents have shown pseudo-second-order kinetics and Langmuir adsorption mechanism. Nanosorbents have shown a specific selectivity for heavy metal ions with a selectivity order of $Ni^{2+} < Co^{2+} < Cd^{2+} < Pb^{2+} < Zn^{2+} < Cu^{2+}$ with individual adsorption capacities 7.94, 15.42, 17.80, 49.46, 56.15, and 66.54 mg g^{-1} and no significant response for common interfering metal ions (Na^+, K^+, Mg^{2+}, and Ca^{2+}), which generally coexist with all natural sources of water,

DOI: 10.1021/acsami.8b17141
ACS Appl. Mater. Interfaces XXXX, XXX, XXX−XXX

contaminated water, and industrial waste. Competitive heavy metal adsorption studies with mixed matrix of all of these ions have exhibited selectivity trend almost similar to individual adsorption performance and nearly complete removal capability for three heavy metal ions (Pb^{2+}, Zn^{2+}, and Cu^{2+}). PS–nanosorbent composite beads have shown explicit selectivity and adequate removal performance for heavy metal ions even in the presence of common interfering metal ions similar to pure nanosorbent.

AUTHOR INFORMATION

Corresponding Authors

*E-mail: hitesh_analytical@yahoo.com, htsaravaia@csmcri.res.in. Tel: +91 2782567760 ext. 6840 (H.S.).
*E-mail: hgupta@cimap.res.in, hhariom.82@gmail.com (H.G.).

ORCID

Hitesh Saravaia: 0000-0003-2811-1469
Vaibhav Kulshrestha: 0000-0003-3980-8843

Present Address

†CSIR-Central Institute of Medicinal and Aromatic Plants, Near Kukrail Picnic Spot, Lucknow 226015, Uttar Pradesh, India (H.G.).

Notes

The authors declare no competing financial interest.

ACKNOWLEDGMENTS

CSIR-CSMCRI Communication No. PRIS/049/2018. The authors thank Rajesh Patidar, Shailendra, Gopal Ram Bhadu, Jayesh Chaudhary, Vinod Agrawal, and Satyaveer of AESD & CIF of CSMCRI for helpful assistance in characterization. V.K. acknowledges SERB, DST New Delhi, for providing financial support.

REFERENCES

(1) Sun, H.; Jiang, J.; Xiao, Y.; Du, J. Efficient Removal of Polycyclic Aromatic Hydrocarbons, Dyes, and Heavy Metal Ions by a Homopolymer Vesicle. *ACS Appl. Mater. Interfaces* **2018**, *10*, 713–722.

(2) Tchounwou, P. B.; Yedjou, C. G.; Patlolla, A. K.; Sutton, D. J. Heavy Metals Toxicity and the Environment. In *Molecular, Clinical and Environmental Toxicology*; Springer: Basel, 2012; Vol. *101*, pp 133–164.

(3) Schwarzenbach, R. P.; Egli, T.; Hofstetter, T. B.; Von Gunten, U.; Wehrli, B. Global Water Pollution and Human Health. *Annu. Rev. Environ. Resour.* **2010**, *35*, 109–136.

(4) Fu, F.; Wang, Q. Removal of Heavy Metal Ions from Wastewaters: A Review. *J. Environ. Manage.* **2011**, *92*, 407–418.

(5) Dudgeon, D.; Arthington, A. H.; Gessner, M. O.; Kawabata, Z. I.; Knowler, D. J.; Leveque, C.; Naiman, R. J.; Prieur-Richard, A. H.; Soto, D.; Stiassny, M. L. J.; Sullivan, C. A. Freshwater Biodiversity: Importance, Threats, Status and Conservation Challenges. *Biol. Rev.* **2006**, *81*, 163–182.

(6) Montgomery, M. A.; Elimelech, M. Water and Sanitation in Developing Countries: Including Health in the Equation. *Environ. Sci. Technol.* **2007**, *41*, 17–24.

(7) Shah, A.; Shahzad, S.; Munir, A.; Nadagouda, M. N.; Khan, G. S.; Shams, D. F.; Dionysiou, D. D.; Rana, U. A. Micelles as Soil and Water Decontamination Agents. *Chem. Rev.* **2016**, *116*, 6042–6074.

(8) Theophanides, T.; Anastassopoulou, J. Copper and carcinogenesis. *Crit. Rev. Oncol.* **2002**, *42*, 57–64.

(9) Strachan, S. Trace Elements. *Curr. Anaesth. Crit. Care* **2010**, *21*, 44–48.

(10) Szewczyk, B. Zinc Homeostasis and Neurodegenerative Disorders. *Front. Aging Neurosci.* **2013**, *5*, No. 33.

(11) Lemire, J.; Mailloux, R.; Appanna, V. D. Zinc Toxicity Alters Mitochondrial Metabolism and Leads to Decreased ATP Production in Hepatocytes. *J. Appl. Toxicol.* **2008**, *28*, 175–182.

(12) Das, K. K.; Das, S. N.; Dhundasi, S. A. Nickel, Its Adverse Health Effects & Oxidative Stress. *Indian J. Med. Res.* **2008**, *128*, 412–425.

(13) Leikauf, G. D.; McDowell, S. A.; Wesselkamper, S. C.; Hardie, W. D.; Leikauf, J. E.; Korfhagen, T. R.; Prows, D. R. Acute Lung Injury: Functional Genomics and Genetic Susceptibility. *Chest* **2002**, *121*, 70S–75S.

(14) Ge, Y.; Bruno, M.; Haykal-Coates, N.; Wallace, K.; Andrews, D.; Swank, A.; Winnik, W.; Ross, J. A. Proteomic Assessment of Biochemical Pathways That Are Critical to Nickel-Induced Toxicity Responses in Human Epithelial Cells. *PLoS One* **2016**, *11*, No. e0162522.

(15) Wani, A. L.; Ara, A.; Usmani, J. A. Lead Toxicity: A Review. *Interdiscip. Toxicol.* **2015**, *8*, 55–64.

(16) Hooser, S. B. In *Veterinary Toxicology*, 3rd ed.; Gupta, R. C., Ed.; Elsevier: Academic Press, 2018; Chapter 24, pp 417–421.

(17) Weiss, B.; Landrigan, P. J. The Developing Brain and the Environment: An Introduction. *Environ. Health Perspect.* **2000**, *108*, 373–374.

(18) *Guidelines for Drinking-water Quality*, 4th ed.; World Health Organization: Geneva, 2017.

(19) Dabrowski, A.; Hubicki, Z.; Podkoscielny, P.; Robens, E. Selective Removal of the Heavy Metal Ions from Waters and Industrial Wastewaters by Ion-Exchange Method. *Chemosphere* **2004**, *56*, 91–106.

(20) Ray, P. Z.; Shipley, H. J. Inorganic Nano-Adsorbents for the Removal of Heavy Metals and Arsenic: A Review. *RSC Adv.* **2015**, *5*, No. 29885.

(21) Blöcher, C.; Dorda, J.; Mavrov, V.; Chmiel, H.; Lazaridis, N. K.; Matis, K. A. Hybrid Flotation-Membrane Filtration Process for the Removal of Heavy Metal Ions from Wastewater. *Water Res.* **2003**, *37*, 4018–4026.

(22) Rao, Z.; Feng, K.; Tang, B.; Wu, P. Surface Decoration of Amino-Functionalized Metal–Organic Framework/Graphene Oxide Composite onto Polydopamine-Coated Membrane Substrate for Highly Efficient Heavy Metal Removal. *ACS Appl. Mater. Interfaces* **2017**, *9*, 2594–2605.

(23) Blowes, D. W.; Ptacek, C. J.; Jambor, J. L. In-Situ Remediation of Cr(VI)-Contaminated Groundwater Using Permeable Reactive Walls: Laboratory Studies. *Environ. Sci. Technol.* **1997**, *31*, 3348–3357.

(24) Wang, J.; Chen, C. Biosorption of Heavy Metals by *Saccharomyces cerevisiae*: A Review. *Biotechnol. Adv.* **2006**, *24*, 427–451.

(25) Feng, Y.; Yang, L.; Liu, J.; Logan, B. E. Electrochemical Technologies for Wastewater Treatment and Resource Reclamation. *Environ. Sci.: Water Res. Technol.* **2016**, *2*, 800–831.

(26) Lu, F.; Astruc, D. Nanomaterials for Removal of Toxic Elements from Water. *Coord. Chem. Rev.* **2018**, *356*, 147–164.

(27) Liu, X.; Hu, Q.; Fang, Z.; Zhang, X.; Zhang, B. Magnetic Chitosan Nanocomposites: A Useful Recyclable Tool for Heavy Metal Ion Removal. *Langmuir* **2009**, *25*, 3–8.

(28) Zhao, T.; Yao, Y.; Wang, M.; Chen, R.; Yu, Y.; Wu, F.; Zhang, C. Preparation of MnO_2-Modified Graphite Sorbents from Spent Li-Ion Batteries for the Treatment of Water Contaminated by Lead, Cadmium, and Silver. *ACS Appl. Mater. Interfaces* **2017**, *9*, No. 25369.

(29) Wei, X.; Sugumaran, P.; Peng, J. E.; Liu, X. L.; Ding, J. Low-Field Dynamic Magnetic Separation by Self-Fabricated Magnetic Meshes for Efficient Heavy Metal Removal. *ACS Appl. Mater. Interfaces* **2017**, *9*, No. 36772.

(30) Qu, L.; Jia, J.; Shi, H.; Luo, Z. One-step Synthesis of Fe_3O_4/carboxylate-rich Carbon Composite and Its Application for Cu(II) Removal. *New J. Chem.* **2016**, *40*, 2895–2903.

DOI: 10.1021/acsami.8b17141
ACS Appl. Mater. Interfaces XXXX, XXX, XXX–XXX

(31) Xu, P.; Zeng, G. M.; Huang, D. L.; Lai, C.; Zhao, M. H.; Wei, Z.; Li, N. J.; Huang, C.; Xie, G. X. Adsorption of Pb(II) by Iron Oxide Nanoparticles Immobilized *Phanerochaete chrysosporium*: Equilibrium, Kinetic, Thermodynamic and Mechanisms Analysis. *Chem. Eng. J.* **2012**, *203*, 423−431.
(32) Qin, L.; Yan, L.; Chen, J.; Liu, T.; Yu, H.; Du, B. Enhanced Removal of Pb^{2+}, Cu^{2+}, and Cd^{2+} by Amino-Functionalized Magnetite/Kaolin Clay. *Ind. Eng. Chem. Res.* **2016**, *55*, 7344−7354.
(33) Zhang, J.; Han, J.; Wang, M.; Guo, R. Fe_3O_4/PANI/MnO_2 Core−Shell Hybrids as Advanced Adsorbents for Heavy Metal Ions. *J. Mater. Chem. A* **2017**, *5*, 4058−4066.
(34) Zhang, Q.; Du, Q.; Jiao, T.; Teng, J.; Sun, Q.; Peng, Q.; Chen, X.; Gao, F. Accelerated Sorption Diffusion for Cu(II) Retention by Anchorage of Nano-zirconium Dioxide onto Highly charged Polystyrene Material. *Sci. Rep.* **2015**, *5*, No. 10646.
(35) Freire, M.; Kosova, N. V.; Jordy, C.; Chateigner, D.; Lebedev, O. I.; Maignan, A.; Pralong, V. A New Active Li−Mn−O Compound for High Energy Density Li-ion Batteries. *Nat. Mater.* **2016**, *15*, 173−177.
(36) Kim, Y. Lithium Nickel Cobalt Manganese Oxide Synthesized Using Alkali Chloride Flux: Morphology and Performance as a Cathode Material for Lithium Ion Batteries. *ACS Appl. Mater. Interfaces* **2012**, *4*, 2329−2333.
(37) Chen, M.; Chen, D.; Liao, Y.; Zhong, X.; Li, W.; Zhang, Y. Layered Lithium-Rich Oxide Nanoparticles Doped with Spinel Phase: Acidic Sucrose-Assistant Synthesis and Excellent Performance as Cathode of Lithium Ion Battery. *ACS Appl. Mater. Interfaces* **2016**, *8*, 4575−4584.
(38) Saravaia, H.; Gupta, H.; Kulshrestha, V. Single Step Synthesis of a Magnesium Doped Lithium Manganese Oxide Ion Sieve Nanomaterial and a SPES/ion Sieve Composite Membrane for the Separation of Lithium. *RSC Adv.* **2016**, *6*, No. 106980.
(39) Chitrakar, R.; Kanoh, H.; Miyai, Y.; Ooi, K. A New Type of Manganese Oxide (MnO_2,0·$5H_2O$) Derived from $Li_{1.6}Mn_{1.6}O_4$ and Its Lithium Ion-Sieve Properties. *Chem. Mater.* **2000**, *12*, 3151−3157.
(40) Ryu, T.; Haldorai, Y.; Rengaraj, A. K.; Shin, J.; Hong, H.-J.; Lee, G. W.; Han, Y.-K.; Huh, Y. S.; Chung, K.-S. Recovery of Lithium Ions from Seawater Using a Continuous Flow Adsorption Column Packed with Granulated Chitosan-Lithium Manganese Oxide. *Ind. Eng. Chem. Res.* **2016**, *55*, 7218−7225.
(41) Chitrakar, R.; Makita, Y.; Ooi, K.; Sonoda, A. Magnesium-Doped Manganese Oxide with Lithium Ion-Sieve Property: Lithium Adsorption from Salt Lake Brine. *Bull. Chem. Soc. Jpn.* **2013**, *86*, 850−855.
(42) Jiang, L.; Ye, Q.; Chen, J.; Chen, Z.; Gu, Y. Preparation of Magnetically Recoverable Bentonite-Fe_3O_4-MnO_2 Composite Particles for Cd(II) Removal from Aqueous Solutions. *J. Colloid Interface Sci.* **2018**, *513*, 748−759.
(43) Warner, C. L.; Chouyyok, W.; Mackie, K. E.; Neiner, D.; Saraf, L. V.; Droubay, T. C.; Warner, M. G.; Addleman, R. S. Manganese Doping of Magnetic Iron Oxide Nanoparticles: Tailoring Surface Reactivity for a Regenerable Heavy Metal Sorbent. *Langmuir* **2012**, *28*, 3931−3937.
(44) Lee, S.-M.; Kim, W.-G.; Laldawngliana, C.; Tiwari, D. Removal Behavior of Surface Modified Sand for Cd(II) and Cr(VI) from Aqueous Solutions. *J. Chem. Eng. Data* **2010**, *55*, 3089−3094.
(45) Qin, Q.; Wang, Q.; Fu, D.; Ma, J. An Efficient Approach for Pb(II) and Cd(II) Removal using Manganese Dioxide formed in Situ. *Chem. Eng. J.* **2011**, *172*, 68−74.
(46) Su, Q.; Pan, B.; Pan, B.; Zhang, Q.; Zhang, W.; Lv, L.; Wang, X.; Wu, J.; Zhang, Q. Fabrication of Polymer-supported Nanosized Hydrous Manganese Dioxide (HMO) for Enhanced Lead Removal from Waters. *Sci. Total Environ.* **2009**, *407*, 5471−5477.
(47) Zhang, H.; Wu, A.; Fu, H.; Zhang, L.; Liu, H.; Zheng, S.; Wan, H.; Xu, Z. Efficient Removal of Pb(II) Ions using Manganese Oxides: The Role of Crystal Structure. *RSC Adv.* **2017**, *7*, No. 41228.
(48) Xiong, Y.; Lu, X.; Tao, H. Selective Adsorption of Lead (II) Ions by a Manganese Dioxides Loaded Adsorption Resin. *Desalin. Water Treat.* **2016**, *57*, 2018−2027.
(49) Kanungo, S. B.; Tripathy, S. S.; Mishra, S. K.; Sahoo, B.; Rajeev. Adsorption of Co^{2+}, Ni^{2+}, Cu^{2+}, and Zn^{2+} onto Amorphous Hydrous Manganese Dioxide from Simple (1−1) Electrolyte Solution. *J. Colloid Interface Sci.* **2004**, *269*, 11−21.
(50) Kanungo, S. B.; Tripathy, S. S.; Rajeev. Adsorption of Co, Ni, Cu, and Zn on Hydrous Manganese Dioxide from Complex Electrolyte Solutions Resembling Sea Water in Major Ion Content. *J. Colloid Interface Sci.* **2004**, *269*, 1−10.
(51) Su, Q.; Pan, B.; Wan, S.; Zhang, W.; Lv, L. Use of Hydrous Manganese Dioxide as a Potential Sorbent for Selective Removal of Lead, Cadmium, and Zinc Ions from Water. *J. Colloid Interface Sci.* **2010**, *349*, 607−612.
(52) Tseng, T. K.; Wang, L.; Chu, H. High-Temperature Cleaning for Chlorine-Containing Coal Gas by Supported Manganese Oxide Sorbent. *Aerosol Air Qual. Res.* **2012**, *12*, 961−971.
(53) Singh, P.; Sil, A.; Nath, M.; Ray, S. Synthesis and characterization of $Li[Mn_{2-x}\ Mg_x]O_4$ (x = 0.0−0.3) prepared by sol-gel synthesis. *Ceram. Silik.* **2010**, *54*, 38−46.
(54) Zhang, Y.; Su, Z.; Yao, X.; Wang, Y. Synthesis and Electrochemical Properties of Monoclinic Fluorine-doped Lithium Manganese Oxide ($Li_xMnO_{2-y}F_y$) for Lithium Secondary batteries. *RSC Adv.* **2015**, *5*, No. 90150.
(55) Li, L.-X.; Xu, D.; Li, X.-Q.; Liu, W.-C.; Jia, Y. Excellent Fluoride Removal Properties of Porous Hollow MgO Microspheres. *New J. Chem.* **2014**, *38*, 5445−5452.
(56) Shaju, K. M.; Bruce, P. G. A Stoichiometric Nano-LiMn2O4 Spinel Electrode Exhibiting High Power and Stable Cycling. *Chem. Mater.* **2008**, *20*, 5557−5562.
(57) Ge, F.; Li, M.-M.; Ye, H.; Zhao, B.-X. Effective Removal of Heavy Metal Ions Cd^{2+}, Zn^{2+}, Pb^{2+}, Cu^{2+} from Aqueous Solution by Polymer-Modified Magnetic Nanoparticles. *J. Hazard. Mater.* **2012**, *211−212*, 366−372.
(58) Kumar, K. V. Linear and Non-linear Regression Analysis for the Sorption Kinetics of Methylene Blue onto Activated Carbon. *J. Hazard. Mater.* **2006**, *B137*, 1538−1544.
(59) Hao, L.; Desai, M. K.; Wang, P.; Valiyaveettil, S. Successive Extraction of As(V), Cu(II), and P(V) Ions from Water Using Surface Modified Ghee Residue Protein. *ACS Sustainable Chem. Eng.* **2017**, *5*, 3742−3750.
(60) McKay, G.; Blair, H. S.; Gardner, J. R. Adsorption of Dyes on Chitin. I. Equilibrium Studies. *J. Appl. Polym. Sci.* **1982**, *27*, 3043−3057.
(61) Ok, Y. S.; Yang, J. E.; Zhang, Y.-S.; Kim, S.-J.; Chung, D.-Y. Heavy Metal Adsorption by a Formulated Zeolite-Portland Cement Mixture. *J. Hazard. Mater.* **2007**, *147*, 91−96.
(62) Sahoo, J. K.; Kumar, A.; Rout, L.; Rath, J.; Dash, P.; Sahoo, H. An Investigation of Heavy Metal Adsorption by Hexa-Dentate Ligand-Modified Magnetic Nanocomposites. *Sep. Sci. Technol.* **2018**, *53*, 863−876.
(63) Bulgariu, L.; Bulgariu, D.; Macoveanu, M. Adsorptive Performances of Alkaline Treated Peat for Heavy Metal Removal. *Sep. Sci. Technol.* **2011**, *46*, 1023−1033.
(64) Xie, Z. H.; Xie, F. Z.; Guo, L. Q.; Lin, X. C.; Chen, G. N. Thioacetamide Chemically Immobilized on Silica Gel as a Solid Phase Extractant for the Extraction and Preconcentration of Copper(II), Lead(II), and Cadmium(II). *J. Sep. Sci.* **2005**, *28*, 462−470.
(65) Lam, K. F.; Yeung, K. L.; Mckay, G. Efficient Approach for Cd^{2+} and Ni^{2+} Removal and Recovery Using Mesoporous Adsorbent with Tunable Selectivity. *Environ. Sci. Technol.* **2007**, *41*, 3329−3334.
(66) Zhou, D.; Zhanga, L.; Zhoua, J.; Guo, S. Cellulose/Chitin Beads for Adsorption of Heavy Metals in Aqueous Solution. *Water Res.* **2004**, *38*, 2643−2650.
(67) Badruddoza, A. Z. M.; Tay, A. S. H.; Tan, P. Y.; Hidajat, K.; Uddin, M. S. Carboxymethyl-β-cyclodextrin Conjugated Magnetic Nanoparticles as Nano-Adsorbents for Removal of Copper ions: Synthesis and Adsorption Studies. *J. Hazard. Mater.* **2011**, *185*, 1177−1186.
(68) Ciesielczyk, F.; Bartczak, P.; Klapiszewski, Ł.; Jesionowski, T. Treatment of Model and Galvanic Waste Solutions of Copper(II)

DOI: 10.1021/acsami.8b17141
ACS Appl. Mater. Interfaces XXXX, XXX, XXX−XXX

Ions using a Lignin/Inorganic Oxide Hybrid as an Effective Sorbent. *J. Hazard. Mater.* **2017**, *328*, 150−159.
(69) Perera, V. S.; Wickramaratne, N. P.; Jaroniec, M.; Huang, S. D. A Highly Efficient and Extremely Selective Intracellular Copper Detoxifying Agent Based on Nanoparticles of $ZnMoS_4$. *J. Mater. Chem. B* **2014**, *2*, 257−261.
(70) Ozmen, M.; Can, K.; Arslan, G.; Tor, A.; Cengeloglu, Y.; Ersoz, M. Adsorption of Cu(II) from Aqueous Solution by using Modified Fe_3O_4 Magnetic Nanoparticles. *Desalination* **2010**, *254*, 162−169.
(71) Kim, E.-J.; Lee, C.-S.; Chang, Y.-Y.; Chang, Y.-S. Hierarchically Structured Manganese Oxide-Coated Magnetic Nanocomposites for the Efficient Removal of Heavy Metal Ions from Aqueous Systems. *ACS Appl. Mater. Interfaces* **2013**, *5*, 9628−9634.
(72) Badruddoza, A. Z. M.; Shawon, Z. B. Z.; Tay, W. J. D.; Hidajat, K.; Uddin, M. S. Fe_3O_4/Cyclodextrin Polymer Nanocomposites for Selective Heavy Metals Removal from Industrial Waste Water. *Carbohydr. Polym.* **2013**, *91*, 322−332.
(73) Li, N.; Li, X.; Wang, C.; Shi, X.; Liu, J. Desorption of Cd (II) from Tourmaline at Acidic Conditions: Kinetics, Equilibrium and Thermodynamics. *J. Environ. Chem. Eng.* **2016**, *4*, 30−36.

DOI: 10.1021/acsami.8b17141
ACS Appl. Mater. Interfaces XXXX, XXX, XXX−XXX